Application of a Novel Miniaturized Histopathologic Microscope for Ex Vivo Identifying Cerebral Glioma Margins Rapidly During Surgery: A Parallel Control Study

Weichi Wu, MD, Baoshu Xie, MD, PhD,* Xiaowei Zhang, MD,* Chen Zheng, MD,* Huixin Sun, MD,* Mingyang Jiang, MD,* Tiefeng Hu, MD,† Xinman Liu, MD,* Nu Zhang, MD, PhD,* and Kejun He, MD**

Purpose: The purpose of our study is to assess the clinical performance of the DiveScope, a novel handheld histopathologic microscope in rapidly differentiating glioma from normal brain tissue during neurosurgery.

Methods: Thirty-two ex vivo specimens from 18 patients were included in the present study. The excised suspicious tissue was sequentially stained with sodium fluorescein and methylene blue and scanned with DiveScope during surgery. The adjacent tissue was sent to the department of pathology for frozen section examination. They would eventually be sent to the pathology department later for hematoxylin and eosin staining for final confirmation. The positive likelihood ratio, negative likelihood ratio, sensitivity, specificity, and area under the curve of the device were calculated. In addition, the difference in time usage between DiveScope and frozen sections was compared for the initial judgment.

Results: The sensitivity and specificity of the DiveScope after analyzing hematoxylin and eosin -staining sections, were 88.29% and 100%, respectively. In contrast, the sensitivity and specificity of the frozen sections histopathology were 100% and 75%, respectively. The area under the curve of the DiveScope and the frozen sections histopathology was not significant ($P = 0.578$). Concerning time usage, DiveScope is significantly much faster than the frozen sections histopathology no matter the size of tissue.

Conclusion: Compared with traditional pathological frozen sections, DiveScope was faster and displayed an equal accuracy for judging tumor margins intraoperatively.

Key Words: DiveScope, glioma, histopathology, surgical margins

(*J Craniofac Surg* 2023;00: 000–000)

From the *Department of Neurosurgery, Institute of Precision Medicine, the First Affiliated Hospital of Sun Yat-sen University, Guangdong Provincial Key Laboratory of Brain Function and Disease, Sun Yat-sen University, Guangzhou, Guangdong, China; and †Yale School of Medicine, New Haven, CT.

Received August 30, 2023.

Accepted for publication September 11, 2023.

Address correspondence and reprint requests to Nu Zhang, MD, PhD (e-mail: zhangnu2@mail.sysu.edu.cn), and Kejun He, MD (e-mail: hekejun3@mail.sysu.edu.cn), Department of Neurosurgery The First Affiliated Hospital of Sun Yat-sen University, No 58, Zhongshan 2 Road Guangzhou, Guangdong Province 510080, China

W.W., B.X., and X.Z. contributed equally.

W.W., B.X., N.Z., and K.H. conceived and designed research. N.Z. led the project. W.W., B.X., X.Z., C.Z., T.H. performed experiments. W.W., H.S., and X.L. performed data analysis and wrote the paper. All authors read and approved the final manuscript.

The datasets generated or analyzed during this study are included in this published article and its supplementary information files.

The protocol for the animal experiments in this study was approved by the institutional review board of Gateway Medical Innovation Center ("Gateway" for short) (IACUC: SH2022-03004). All the human tissues were obtained from the Department of Neurosurgery at the First Affiliated Hospital of Sun Yat-sen University. Tissues were obtained after patients' written consent under a protocol approved by the institutional review board of the First Affiliated Hospital of Sun Yat-sen University (No. [2020]322).

Written consent is obtained from all patients according to our hospital-approved protocol.

This work was supported by the National Natural Science Foundation of China 82001307 (to B.X.) and 81802484 (to K.H.), and the Natural Science Foundation of Guangdong Province 2018A030313549 (to K. H.) and Guangdong Basic and Applied Basic Research Foundation 2019A1515110460 (to B.X.).

The authors report no conflicts of interest.

Supplemental Digital Content is available for this article. Direct URL citations are provided in the HTML and PDF versions of this article on the journal's website, www.jcraniofacialsurgery.com.

ISSN: 1049-2275

DOI: 10.1097/SCS.0000000000009787

Gliomas are the primary malignant tumor of the central nervous system,[1] especially high-grade gliomas, which are responsible for the highest mortality rate.[2] The strongest prognostic factor for glioma is residual cavity tumor burden.[3] Petrecca et al[4] have demonstrated that 90% of glioblastoma will recur in situ within 2 years despite gross total resection. Currently, the conventional treatment for glioma is maximal surgical resection with preservation of neurologic function.[5–8] Hence, it is vital to precisely and swiftly define the boundaries of the glioma during surgery. This is necessary to minimize the amount of remaining tumor tissue and prevent over excision, which can lead to neurological deficits.[9]

The practice of utilizing frozen pathology is a common and traditional approach within the field of neurosurgery.[10] Because

this procedure requires substantial time and exertion, rapid identification is unattainable, particularly in cases where there is a sizable residual cavity and multiple sites must be sampled.[11] Over recent decades, surgical techniques for delineating brain lesions have evolved greatly.[9] Microendoscope systems similar to Divescope such as Endoscopic Raman spectroscopy,[12] Multiphoton endomicroscopy,[13] and Confocal endomicroscopy.[14] The depth of penetration of Divescope Endomicroscope being 50 μm,[15] shows its suitability as a cell morphology visualizer.

Herein, we present preliminary evidence of the efficacy of real-time visualization of brain tumors using the prototype DiveScope fluorescence imaging device for clinical applications. The DiveScope is an innovative epifluorescence microscope that comprises an image acquisition system, a light-emitting diode (LED) light source, camera readout, and a monitor. The LED light source emits blue light onto the tissue surface through light-transmitting bundles. The emitted green light is received by the microscopic imaging amplification system to enhance the signals. The camera system collects and processes the signals, which are eventually transmitted to the monitor in the form of an image (1980×1080 pixels). The lens is equipped with optical anti-shake performance, providing a resolution of up to 50 μm and a frame rate of up to 60 frames/s. Our work aimed to demonstrate the device's feasibility in detecting intracranial residual walls in live swine in vivo. We then conducted a human ex vivo study of glioma margin assessment to compare the diagnostic accuracy, consistency, and timeliness between the DiveScope and frozen section.

MATERIALS AND METHODS

Patient Selection

Our prospective ex vivo cohort study enrolled 40 consecutive patients with 54 samples from November 2021 to May 2022 in the Department of Neurosurgery at the First Affiliated Hospital of Sun Yat-sen University. Inclusion criteria: (1) Diagnosis of glioma, (2) Tumor size larger than 1 cm based on imaging examination, (3) Scheduled for total tumor resection surgery. After these criteria, 22 cases were initially considered. However, 4 cases were excluded due to an inability to complete the gold standard test. Consequently, a total of 18 cases, comprising 32 samples, fulfilled the statistical requirements and were eligible for analysis. Written consent was obtained from all patients under a protocol approved by the institutional review board of the First Affiliated Hospital of Sun Yat-sen University (No. [2020]322). For more detailed patient demographics, see Supplemental Table 1, Supplemental Digital Content 1, http://links.lww.com/SCS/F573.

Specimen Preparation

Specimen Preparation Procedure: Tissue samples are procured from the peritumoral region and tumor margins. Before staining, the samples are segmented into 3 sections. These sections are subsequently dispatched to Digital Pathology (DS), Frozen Pathology, and Paraffin Pathology for staining and processing.

DS, Frozen, and Paraffin Pathology Slide Review Protocol:

Slide review is undertaken using 3 distinct approaches: DS interpretation by a neurosurgeon, evaluation by a frozen pathology specialist, and assessment by a paraffin pathology (HE) expert. These evaluations are conducted consecutively, and the outcomes are meticulously documented. The HE findings serve as the reference standard against which DS and frozen pathology results are juxtaposed. In addition, the time required for DS and frozen pathology assessments is logged and subjected to comparative analysis (Fig. 1).

During the dyeing process, we began by thoroughly mixing 0.5 mL of standard fluorescein sodium (3 mL: 0.6 g) with 49.5 mL of 0.9% sodium chloride, creating a solution of 0.2% sodium fluorescein. Subsequently, we extracted 2 mL of the mixture and placed it in a container. The sample was then subjected to staining using the diluted sodium fluorescein solution for 30 seconds. After the staining, the sample underwent a thorough rinse with 0.9% sodium chloride 3 times. After this, the sample was infiltrated with a 1% methylene blue solution for 90 seconds, and then it was washed with 0.9% sodium chloride 3 times before being observed under the DiveScope.

Diagnosis of the Pathologic Images

The diagnostic process involving both DiveScope and frozen sections histopathology is conducted under a double-blind protocol. In addition, the interpreters are kept unaware of the overall impression regarding the residual tumor status within the cavity. The margin status was divided into negative and positive by whether there are obvious atypical cells or not. Atypic cells are typically characterized by increased density, enhanced nuclear staining, irregular nuclear shapes, and/or enlarged nuclei. The interpretation standard of DiveScope and histopathology is the same. Routine pathology diagnosis was used as the reference. Before the trial, 2 surgeons were trained for an hour with 30 DiveScope images of glioma margins. The images were provided by Max Act Precision Instruments. A conclusive diagnosis was reached through collaborative consultation. In addition, a dedicated neuropathologist was responsible for frozen section histopathology interpretation. Meanwhile, we will measure the time span from the initiation of staining to the issuance of the initial report for both diagnostic methods.

Statistical Analysis

All statistical analyses were conducted by IBM SPSS Statistics Version 26.0 and the Medical statistical software package V19.0.4. Postoperative routine pathology results of patients were used as the benchmark reference. $P < 0.05$ are considered statistical differences. The data analysis in our work includes 3 parts. In first part, diagnostic accuracy was compared between DiveScope and frozen modalities using 2-sample Z tests. In this part, area under the curve (AUC), Sensitivity, specificity, positive likelihood ratio, and negative likelihood ratio were calculated with 95% CI. In the second part, kappa coefficients were computed to assess the concordance of the DiveScope findings, frozen section histopathology analysis, and results from the permanent pathologic paraffin assessment. Moving on to the third part, we evaluated the disparity in time consumption between DiveScope and intraoperative frozen section pathologic examinations for the initial evaluation.

RESULTS

The Structure of the Final Product of the DiveScope with a Superb Resolution to Visualize Sub-Micron Organelles

In the final iteration of the DiveScope, the surgical microscope assembly and processing system encompass the core structure of an imaging platform, a camera readout mechanism, a microscopy unit, a distal hood, an electrical conduit, a display screen, and an LED illumination source (Fig. 2A).

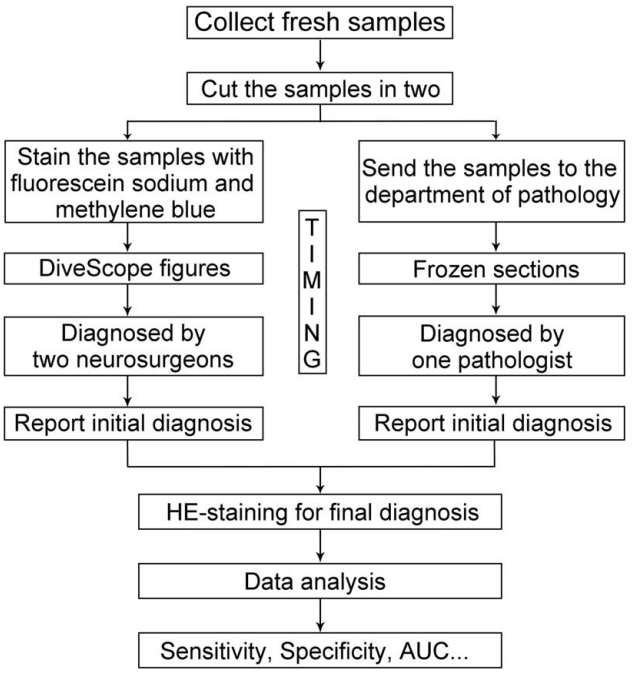

FIGURE 1. Workflow chart. AUC indicates area under the curve.

With exceptional resolution, the DiveScope enabled visualization of the resolution test chart and sub-micron cellular structures, such as nuclei, nucleoli, and cytosol, during in vitro imaging. This capability aligns with the current advancements in microscopy techniques (Fig. 2B, C).

Performance of the Handheld Microscope in Clinical Application

Patient demographic and clinical parameters were extracted through chart reviews (Supplemental Table 1, Supplemental Digital Content 1, http://links.lww.com/SCS/F573). In every case, DiveScope successfully detected and differentiated fluorescent tissues at the resection cavity's margins after completion of the microscopic resection (Fig. 3).

Diagnostic Accuracy of the DiveScope in Resection Margins

As demonstrated in Supplemental Table 2, Supplemental Digital Content 1, http://links.lww.com/SCS/F573, the concordance between DiveScope findings and hematoxylin and eosin (HE)-staining pathology results is deemed satisfactory, indicated by a Kappa value of 0.68. Simultaneously, the 2×2 contingency table comparing frozen section pathology to HE-staining pathology is presented in Supplemental Table 3, Supplemental Digital Content 1, http://links.lww.com/SCS/F573, yielding a Kappa value of 0.84.

Next, we directly compared the interpretations from the DiveScope with those from the frozen sections. We calculated diagnostic accuracy measures to evaluate the efficacy of the DiveScope as a novel intraoperative miniaturized histopathologic device (refer to Supplemental Table 4, Supplemental Digital Content 1, http://links.lww.com/SCS/F573). Consequently, 32 samples collected from 18 patients were classified as either tumor or normal tissue using the DiveScope. When considering HE-stained sections as the benchmark reference, the DiveScope exhibited a sensitivity of 88.29% (95% CI: 70.8%–97.6%) and a specificity of 100% (95% CI: 39.8%–100%). In contrast, the frozen sections pathology showed a sensitivity and specificity of 100% (95% CI: 87.7%–100%) and 75% (95% CI: 19.4%–99.4%), respectively.

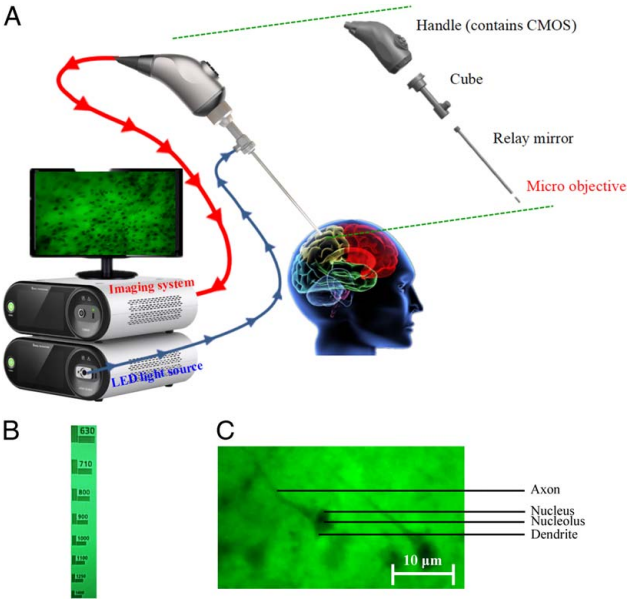

FIGURE 2. Brief introduction to the DiveScope. (A) The architecture of DiveScope, an intraoperative histopathologic microscope, comprises several integral components. The system diagram delineates the core elements, including the imaging system's mainframe, an LED light source, a handle housing a Complementary Metal-Oxide-Semiconductor (CMOS) device, a cube, a relay mirror, a micro-objective, and an associated power cord (omitted from the figure). The optical constituents encompass a CMOS camera, a C-Mount, a fluorescence cube, a relay lens, and a miniature objective. The camera system is fundamentally composed of an image-processing host and the camera apparatus. The operational principle of this camera system revolves around connecting the lens assembly through an optical interface. This facilitates the conversion of optical signals amassed by the lens assembly into digital signals. Subsequently, these signals are fed into the image-processing host for necessary manipulation before being presented on a display. The image-processing host functions as the central control hub, orchestrating the processing of surgical videos and images acquired through the camera. Notably, our device uses a cold light bulb, which operates on akin principles to those governing LEDs. The cold light source operates by channeling power from the module to individual functional units. The program intricacies are integrated into the control board module, which encompasses 3 primary divisions: the Medium Attachment Unit module, the LED driver module, and the dimming module. (B) DiveScope captures imagery of a film resolution chart. (C) Neuron imaging under in vitro conditions is performed utilizing a staining methodology explicated in the "Methods" section of this manuscript.

In addition, the positive likelihood ratio of the DiveScope revealed no false positive cases. Conversely, the negative likelihood ratio was 0.11 (95% CI: 0.037–0.31). Regarding the ROC curve analysis, the AUC values for the DiveScope and the frozen sections were 0.946 and 0.875, respectively (as shown in Fig. 4A). These results demonstrate the diagnostic capabilities of the DiveScope as a novel intraoperative miniaturized histopathologic device in comparison to traditional frozen sections.

Time Consumption

To objectively evaluate the efficiency of the DiveScope in rapid intraoperative pathologic diagnosis, we categorized the samples into 2 groups according to the median diameter of all the tumor samples (0.8 cm) and analyzed the time consumption for DiveScope or frozen sections, respectively (Fig. 4B, C). The results showed that the time consumption for tissue identification

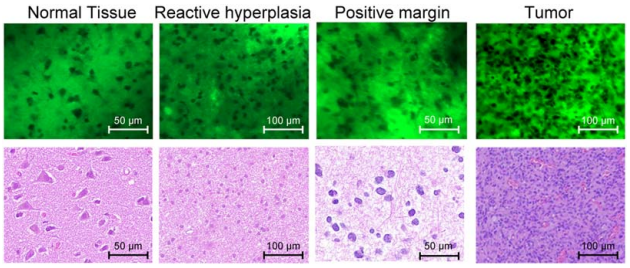

FIGURE 3. Views of the resected human brain tissue through the DiveScope (upper) or hematoxylin and eosin-stained section (lower). In normal tissue, all the neurons are in a sparse and regular cell distribution, with only one large and round nucleus plus a long axon and multiple dendrites. In reactive hyperplasia, the density of the glial cells slightly increased but no atypical cells were found. In positive margin, over 1/50 of the visual field are heterotypic cells which are typically characterized by increased density, enhanced nuclear staining, irregular nuclear shapes, and/or enlarged nuclei. In tumor samples, heterotypic cells nearly filled the visual field. The staining method is stated in the "Experimental Procedure" section of the text.

for the DiveScope is significantly much faster than the frozen sections no matter what size the sample is.

DISCUSSION

Efficiently and precisely detecting the boundaries of infiltrative gliomas poses a fundamental difficulty during glioma surgery.[16] The perfect histopathology system for intraoperative use would offer swift, consistent, and precise diagnostic images to aid in making surgical decisions.[17] Our work demonstrates the potential feasibility of Divescope to distinguish glioma margins from normal tissue with high accuracy and velocity.

The main advantage of DiveScope is OIS anti-shaking design, avoiding image artifacts caused by pulsating blood vessels and artificial shaking. In addition, ensuring its real-time histomorphology feedback with video output of 60 frames/s. It allows tissue and cell structure with subtle nucleoli and nuclei to be obtained at an ultra-high resolution up to 50 μm. Gliomas are characterized by increased cell density, irregular edges, increased bulk, and deep staining nuclear. Reactive gliosis showed increased glial cell density but no atypical cells. Nevertheless, normal brain tissue cells are sparse and evenly distributed.[18] Therefore, it is crucial for surgeons to use devices such as DiveScope to interpret glioma margin intraoperatively.

In human ex vivo experiments, we further verify the diagnostic efficiency of the DiveScope by neurosurgeons. The results indicate that the interpretation accuracy of DiveScope was superior to that of intraoperative frozen sections, although there was no statistical significance. The rationale for this discrepancy is that intraoperative frozen sections are easily disrupted by ice crystals and tissue extrusion during sampling,[19] which significantly impacts frozen section interpretation value. In contrast, DiveScope can circumvent these limitations with a non-invasive probe in real time. In the consistency test, frozen section was found to correlate moderately with DiveScope, with a Kappa value of 0.54 ($P = 0.578$), suggesting that DiveScope's images could be provided to pathologists as an important reference for issuing intraoperative frozen reports in the future, which may substantially improve the accuracy of intraoperative diagnosis. Concerning time effectiveness, the time of DiveScope consumption is much less than frozen reports which may avoid the adverse effects of extending operation time.

To date, there are several kinds of intraoperative marginal exploration have been reported. These techniques are mainly divided into radiography technique, fluorescein-guided surgical technique, and optical technique.[9] The radiography technique only offers macroscopic visibility which is not suitable for principle of maximal resection.[11] Five-aminolevulinic acid fluorescein-guided surgical has become an indispensable surgical technique at many neurosurgical departments. Whereas its negative predictive value is limited in regions with low-density tumor cell infiltration with value widely varied from 22% to 91%.[20] Confocal laser microscopes and Raman spectrometers are the 2 major branches of optics. The former that is, CLE is represented by ZEISS CONVIVO System that identify tumor by histomorphology. However, the probe needs to be affixed on the retractor arm for better quality images even though the handheld use was easier, but the images were of lower quality.[21] This was not the case with Divescope and handheld use produced high quality images (Fig. 4). Martirosyan et al reported that the average usage time of CLE device usage was 15.7 minutes, and 17 seconds and 8 seconds were required to get a diagnostic image in vivo and ex vivo, respectively.[21] In contrast to these findings our usage of Divescope Endomicroscope required average time of 10.7 minutes

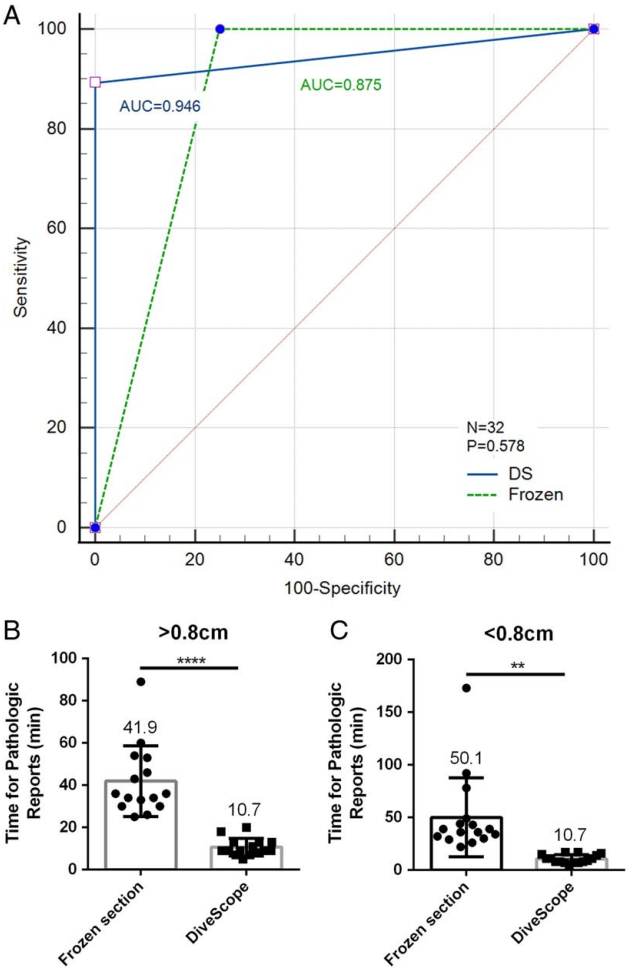

FIGURE 4. The diagnostic accuracy and time consumption of the DiveScope in resection margins. (A) The ROC curve of DiveScope and frozen sections for evaluating tissue edge on brain tumors. (B) In tumor samples with ≥0.8 cm in diameter, DiveScope took 10.7 minutes on average whereas frozen pathology took 41.9 minutes ($P < 0.0001$). (C) In tumor samples with <0.8 cm in diameter, DiveScope took 10.7 minutes on average whereas frozen pathology took 50.1 minutes ($P < 0.01$). AUC indicates area under the curve; ROC, receiver operating characteristic.

(Fig.4). This time efficiency accompanied by sensitivity and specificity benefits and producing higher quality images during handheld application of DiveScope is promising. Raman spectroscopy on the other hand has shown promising application in the accurate diagnosis of cancerous tissues by detecting the molecular space configuration,[17,22] due to the infrequency of Raman scattering events, pixel-by-pixel measurement of a surgical field of view is unfeasible as this quickly leads to imaging times of multiple hours for specimens as small as 1 mm^2.[23,24] Even if they improved the protocol, such approaches still require 12 to 24 min for imaging.[25,26] Considering the intraoperative jitter, it is also limited to applications in vivo.

Limitations

There are some shortcomings in our study. First, the small sample size may result in insufficient results interpretation power. In the forthcoming work, we will continue collecting glioma patients' samples to enhance our evidence. Second, the interpretation of DiveScope images without the involvement of pathologists. We will check for image judgments through a collaborative effort of surgeons and pathologists both in next stage. Furthermore, the pseudo-colored images of DiveScope are highly similar to H&E, but not identical. Thus, successfully interpreting DiveScope images necessitates a learning curve. Additional research on the role of surgeon experience could be considered to optimize training.

CONCLUSION

The handheld microscope DiveScope is an emerging technique with significant potential to detect glioma margin status in vivo and ex vivo with high accuracy and speed. This facilitates real-time decision-making by guiding surgeons to potential positive margins within minutes and allowing operators to adjust the surgical plan in real time.

ACKNOWLEDGMENTS

The authors thank all the contributors to these clinical studies. The authors express our deep gratitude to all principal investigators at the sites where the studies were conducted. The authors also thank Chengzhou He for his writing and editorial assistance.

REFERENCES

1. Jin Z, Yue Q, Duan W, et al. Intelligent SERS navigation system guiding brain tumor surgery by intraoperatively delineating the metabolic acidosis. *Adv Sci (Weinheim)* 2022;9:e2104935
2. Roux A, Zanello M, Simboli GA, et al. Clinico-radio-histo-molecular and neurocognitive characteristics of diffuse gliomas in adolescent and young adults. A comprehensive review. *Oncology* 2023;101:240–251
3. Grabowski MM, Recinos PF, Nowacki AS, et al. Residual tumor volume versus extent of resection: predictors of survival after surgery for glioblastoma. *J Neurosurg* 2014;121:1115–1123
4. Petrecca K, Guiot MC, Panet-Raymond V, et al. Failure pattern following complete resection plus radiotherapy and temozolomide is at the resection margin in patients with glioblastoma. *J Neurooncol* 2013;111:19–23
5. Raco A, Esposito V, Lenzi J, et al. Long-term follow-up of intramedullary spinal cord tumors: a series of 202 cases. *Neurosurgery* 2005;56:972–981
6. Ottenhausen M, Krieg SM, Meyer B, et al. Functional preoperative and intraoperative mapping and monitoring: increasing safety and efficacy in glioma surgery. *Neurosurg Focus* 2015;38:E3
7. Rodríguez-Camacho A, Flores-Vázquez JG, Moscardini-Martelli J, et al. Glioblastoma treatment: state-of-the-art and future perspectives. *Int J Mol Sci* 2022;23:7207
8. Mansouri A, Lai C, Scales D, et al. A phase II pilot randomized controlled trial to assess the feasibility of the "supra-marginal" surgical resection of malignant glioma (G-SUMIT: Glioma supra marginal incision trial) study protocol. *Pilot Feasibility Stud* 2022;8:138
9. Van Hese L, De Vleeschouwer S, Theys T, et al. The diagnostic accuracy of intraoperative differentiation and delineation techniques in brain tumours. *Discov Oncol* 2022;13:123
10. Gould PV, Saikali S. A comparison of digitized frozen section and smear preparations for intraoperative neurotelepathology. *Anal Cell Pathol (Amst)* 2012;35:85–91
11. Pekmezci M, Morshed RA, Chunduru P, et al. Detection of glioma infiltration at the tumor margin using quantitative stimulated Raman scattering histology. *Sci Rep* 2021;11:12162
12. Heng HPS, Shu C, Zheng W, et al. Advances in real-time fiber-optic Raman spectroscopy for early cancer diagnosis: Pushing the frontier into clinical endoscopic applications. *Transl Biophotonics* 2021;3:1–31
13. Dilipkumar A, Al-Shemmary A, Kreiss L, et al. Label-free multiphoton endomicroscopy for minimally invasive in vivo imaging. *Adv Sci (Weinheim)* 2019;6:1801735
14. Pang S, Yao H, Jiang C, et al. Confocal laser endomicroscopy can improve the diagnosis rate and range assessment of patients with conflicting chronic atrophic gastritis results of white light endoscopic and pathological diagnosis. *Front Oncol* 2022;12:809822
15. Zhang Y, Xie M, Xue R, et al. A novel cell morphology analyzer application in head and neck cancer. *Int J Gen Med* 2021;14:9307–9314
16. Leclerc P, Ray C, Mahieu-Williame L, et al. Machine learning-based prediction of glioma margin from 5-ALA induced PpIX fluorescence spectroscopy. *Sci Rep* 2020;10:1462
17. Orringer DA, Pandian B, Niknafs YS, et al. Rapid intraoperative histology of unprocessed surgical specimens via fibre-laser-based stimulated Raman scattering microscopy. *Nat Biomed Eng* 2017;1:0027
18. Rivera-Zengotita M, Yachnis AT. Gliosis versus glioma?: don't grade until you know. *Adv Anat Pathol* 2012;19:239–249
19. Chand P, Amit S, Gupta R, et al. Errors, limitations, and pitfalls in the diagnosis of central and peripheral nervous system lesions in intraoperative cytology and frozen sections. *J Cytol* 2016;33:93–97
20. Hadjipanayis CG, Widhalm G, Stummer W. What is the surgical benefit of utilizing 5-aminolevulinic acid for fluorescence-guided surgery of malignant gliomas? *Neurosurgery* 2015;77:663–673
21. Martirosyan NL, Eschbacher JM, Kalani MY, et al. Prospective evaluation of the utility of intraoperative confocal laser endomicroscopy in patients with brain neoplasms using fluorescein sodium: experience with 74 cases. *Neurosurg Focus* 2016;40:E11
22. Horgan CC, Bergholt MS, Thin MZ, et al. Image-guided Raman spectroscopy probe-tracking for tumor margin delineation. *J Biomed Opt* 2021;26:036002.
23. Pence I, Mahadevan-Jansen A. Clinical instrumentation and applications of Raman spectroscopy. *Chem Soc Rev* 2016;45:1958–1979
24. Hubbard TJE, Shore A, Stone N. Raman spectroscopy for rapid intra-operative margin analysis of surgically excised tumour specimens. *Analyst* 2019;144:6479–6496
25. Kong K, Rowlands CJ, Varma S, et al. Diagnosis of tumors during tissue-conserving surgery with integrated autofluorescence and Raman scattering microscopy. *Proc Natl Acad Sci USA* 2013;110:15189–15194
26. Shipp DW, Rakha EA, Koloydenko AA, et al. Intra-operative spectroscopic assessment of surgical margins during breast conserving surgery. *Breast Cancer Res* 2018;20:69